Aggregation of Oligoarginines at Phospholipid Membranes: Molecular Dynamics Simulations, Time-Dependent Fluorescence Shift, and Biomimetic Colorimetric Assays

Mario Vazdar,*[a,b] Erik Wernersson,[b] Morteza Khabiri,[b] Lukasz Cwiklik,[c,b] Piotr Jurkiewicz,[c] Martin Hof,[c] Ella Mann,[d] Sofiya Kolusheva,[d] Raz Jelinek,[d] and Pavel Jungwirth[b,e]

[a] Division of Organic Chemistry and Biochemistry
Rudjer Bošković Institute
P.O.B. 180, HR-10002 Zagreb, Croatia

[b] Institute of Organic Chemistry and Biochemistry
Academy of Sciences of the Czech Republic
Flemingovo nám. 2, 16610 Prague 6, Czech Republic

[c] J. Heyrovský Institute of Physical Chemistry
Academy of Sciences of the Czech Republic v.v.i.,
Dolejskova 3, 18223 Prague 8, Czech Republic

[d] Department of Chemistry and the Ilse Katz Institute for Nanoscale Science and Technology Beer Sheva 84105, Israel

[e] Department of Physics, Tampere University of Technology
P.O. Box 692, FI-33101 Tampere, Finland

*corresponding author; e-mail: mario.vazdar@irb.hr

Abstract

Time-dependent fluorescence shift method, biomimetic colorimetric assays, and molecular dynamics simulations have been performed in search of explanations why arginine rich peptides with intermediate lengths of about ten amino acids translocate well through cellular membranes, while analogous lysine rich peptides do not. First, we demonstrate that an important factor for efficient peptide adsorption, as the first prerequisite for translocation across the membrane, is the presence of negatively charged phospholipids in the bilayer. Second, we observe a strong tendency of adsorbed arginine (but not lysine) containing peptides to aggregate at the bilayer surface. We suggest that this aggregation of oligoarginines leads to partial disruption of the bilayer integrity due to the accumulated large positive charge at its surface which increases membrane-surface interactions due to the increased effective charge of the aggregates. As a result, membrane penetration and translocation of medium length oligoarginines becomes facilitated in comparison to single arginine and very long polyarginines, as well as to lysine containing peptides.

Keywords: cell penetrating peptides, oligoarginine, molecular dynamics, membranes, fluorescence spectroscopy

1. Introduction

Arginine-rich cell penetrating peptides (CPPs) have drawn a lot of attention due to their ability to readily cross phospholipid membranes[1-4] and deliver various molecular cargos inside the cell, including nucleic acids,[5-7] proteins,[8,9] quantum dots[10-12] and various drugs.[13] It seems that the prinicipal structural requirement for CPPs to effectively penetrate through the phospholipid bilayer is the presence of multiple guanidinium cationic side chain groups which has been described in literature as "arginine magic".[14,15] Remarkably, experimental results obtained by confocal microscopy and flow cytometry have shown that oligoarginines containing six or more amino acids internalize far more efficiently than equally long lysine oligomers.[16] Moreover, the translocation ability for oligoarginines is lowered again for peptides longer than 15 residues and vanishes for even longer polyarginines.

The exact mechanism of translocation is not fully understood. Various mechanistic explanations have been proposed so far such as inverse micelle formation,[1,17,18] electroporation,[19-21] endocytosis,[22-26] and anion mediated energy-independent diffusion through the membrane.[14,27-30] It has been also suggested that arginine-rich CPPs bind to heparin sulfate proteoglycans found on the surface of mammalian cells, which could facilitate their transport through the membrane.[3,31] Recent experiments have shown, however, that nona-arginine translocates also to the proteoglycan deficient cells at temperatures as low as 4 °C questioning thus active endocytosis and proteoglycan mediated transport.[32] This finding supports the notion that direct energy-independent diffusion is at least partially responsible for CPP translocation to the cell interior. In contrast, it has been shown recently that nona-arginines administered in low concentrations of 1 μM neither directly translocate through negatively charged model bilayers nor through Chinese hamster ovary cells at 22 °C, suggesting that nona-arginines enter cells by endocytosis exclusively.[33,34]

A mechanistic description of CPP internalization to the cell interior is thus still incomplete. For example, recent experimental work has revealed that free energy barrier needed for the translocon mediated insertion of arginine residues of transmembrane helices into the endoplasmic reticulum membrane is remarkably small, being only 2.5 kcal mol^{-1}.[35] This value is significantly different from potential of mean force (PMF) calculations which predict that free energy barrier for arginine insertion in the phospholipid bilayer is around 20 kcal mol^{-1}.[36-41] This large difference from the translocon mediated insertion experiment has been explained to some degree by “snorkeling” of transmembrane arginine residues to the cell

membrane interface, which prevents them from residing in the core of the phospholipid bilayer, thus strongly reducing the free energy of insertion observed experimentally.[41] Another recent way of rationalizing the discrepancy assumes that the translocon insertion is actually a nonequilibrium process where the measured energy does not correspond to the free energy difference between translocon and the membrane.[42] Recently, it has been proposed that high concentration and charge density of adsorbed peptides on the membrane surface can destabilize the phospholipid bilayer and induce transient pore formation at a time scale of hundreds of nanoseconds.[43,44] Although this mechanism could explain spontaneous CPP internalization to the cell interior, it was later attributed to a simulation artifact and subsequent simulations have not produced signs of a transient pore formation.[45] Nevertheless, water penetration into the bilayer may still play a role in CPP internalization.[46] Additional theoretical explanations of an energy independent cell entry, apart from the direct penetration mechanism, have been addressed in literature as well. In particular, passive endocytotic internalization via macropinocytosis has been recently proposed.[45,47] This mechanism leads to formation of small vesicles which encapsulate the peptide and subsequently release it into the cell interior and which can also be operative without the need for energy in the form of the ATP/ADP conversion.

The presented theoretical mechanisms have problems in predicting the different cell penetration behavior of positively charged arginine vs. lysine containing peptides, as well as the dependence of the translocation ability on the peptide length. Regardless of the exact mechanism responsible for the cell penetration itself, the first step is the adsorption of the peptide to the bilayer surface and we presume that various adsorption patterns may be directly responsible for different cell penetration behavior of particular CPPs.

In this work, we thus chose to study adsorption of individual arginine (Arg) and lysine (Lys) amino acids, longer oligomers deca-arginine (deca-Arg) and deca-lysine (deca-Lys), and polymeric poly-arginine (poly-Arg) and poly-lysine (poly-Lys) with average length of ca. 50 monomeric units at various model membrane systems using time-dependent fluorescence shift (TDFS) method and biomimetic colorimetric assays, as well as molecular dynamics (MD) simulations.

In TDFS experiments, we followed interactions of these peptides with two bilayer systems – neutral zwitterionic 1-palmitoyl-2-oleoyl-sn-glycero-3-phosphocholine (POPC) vesicles and negatively charged mixed 80 mol % POPC + 20 mol % 1-palmitoyl-2-oleoyl-sn-glycero-3-phosphatidylserine (POPS) vesicles (POPC/POPS). Negatively charged mixed

POPC/POPS vesicles were selected due to the presence of negatively charged lipids in various biological systems..[48,49] For biomimetic colorimetric assays we employed mixed negatively charged vesicles composed of POPC phospholipids and polymerized polydiacetylene (PDA). PDA is a conjugated ene-yne polymer assembly produced upon ultraviolet irradiation of ordered diacetylene monomers (10,12-tricosadiynoic acid).[50] Since their introduction in the early 1970's, PDA systems, primarily vesicles and thin films, have attracted significant scientific and technological interest due to their unique chromatic properties.[51,52] Specifically, PDA matrixes were shown to undergo dramatic visible colorimetric and fluorescence transformations induced by diverse biological and chemical molecules and environmental stimuli, making PDA a powerful constituent in sensing platforms.[53-55] Published studies have demonstrated that PDA vesicles containing zwitterionic lipids constitute reliable models for eukaryotic cell membranes.[54,56] In order to interpret at the molecular level the peptide-vesicle interactions observed experimentally, we performed MD simulations of analogous model peptide-membrane systems (Figure 1).

2. Experimental Section

2.1. Time-dependent fluorescence shift

To experimentally explore the interactions of peptides with model membranes, we employed time-dependent fluorescence shift method (TDFS),[57] in order to monitor local lipid mobility and hydration.[58] TDFS experiments were performed on large unilamellar liposomes composed either of POPC or POPC with POPS. The vesicles were fluorescently labeled with 6-dodecanoyl-2-dimethylaminonaphthalene (Laurdan) and 4-(n-dodecylthiomethyl)-7-(N,N-dimethylamino)coumarin (Dtmac). Steady-state emission spectra and fluorescence decays were used to reconstruct time-resolved emission spectra (TRES). The position of TRES maximum, $\nu(t)$, after electronic excitation at t = 0 s, reflects dipolar relaxation of the probe microenvironment.[59] Analysis of TRES position gives two parameters: 1) $\Delta\nu = \nu(0) - \nu(\infty)$, i.e. the total emission shift, which is directly proportional to the polarity of the microenvironment of Laurdan or Dtmac, and 2) τ, integrated relaxation time, which is a measure of the mobility of the hydrated carbonyls (corresponding to the location of the Laurdan fluorophore) or hydrated phosphates (next to the Dtmac fluorophore), respectively

(Figure 2).[60-63] The time-dependent fluorescence shift (TDFS) method, often referred to as fluorescence solvent relaxation, was described in details elsewhere.[57] Let us mention that the observed changes are usually less pronounced for Dtmac than for Laurdan probe, since the relaxation at the level of Dtmac is faster and thus less precisely described with our time resolution (see the estimated percentage of the experimentally captured relaxation, % obs, in Tables 1 and 2 for Laurdan and Dtmac).[57]

Suspensions of large unilamellar liposomes (LUVs) were prepared as follows. Chloroform solution of POPC, or 80 mol % POPC + 20 mol % POPS mixture (Avanti Polar Lipids, Inc., Alabaster, AL, USA) was mixed with methanol solution of Laurdan (Molecular Probes, Eugene, OR, USA) or Dtmac (synthesized as described in Ref [64]); lipid/dye molar ratio 100:1. Organic solvents were evaporated under stream of nitrogen and then under vacuum for 24 hours. The resulting dry lipid film was suspended in 10 mM Hepes buffer (pH=7.4, 150 mM NaCl, 0.1 mM EDTA). After 4 minutes of continuous stirring the suspension of multilamellar liposomes was extruded through polycarbonate filters with an effective pore diameter of 100 nm (Avestin, Ottawa, Canada). The resulting LUV suspension was mixed with an appropriate amount of amino acid or peptide solution prior to measurement. The amino acid per lipid ratio was always kept constant to 100:1 providing different concentrations of peptides used depending on the peptide length (100 mM for Arg and Lys, 10 mM for deca-Arg and deca-Lys, 1.9 mM for poly-Arg and 2.2 mM for poly-Lys, respectively). L-lysine, L-arginine, poly-L-lysine hydrobromide (MW = 4000-15000) and poly-L-arginine hydrochloride (MW = 5000-15000) were purchased from Sigma-Aldrich (St. Louis, MO, USA), while deca-lysine and deca-arginine (both HCl salts) were obtained from GenScript (Wheelock House, Central, Hong Kong). All peptides and amino acids were used without further purification. Samples were transferred to 1.5 mL quartz cuvettes (Hellma, Müllheim, Germany) with a 1-cm excitation light path and incubated for 30 min at 283 K. Temperature in the cuvette holders was maintained at 283 ± 0.5 K during the measurements using a water-circulating bath. Steady-state emission spectra were collected using a Fluorolog-3 spectrofluorimeter (model FL3-11; Jobin Yvon Inc., Edison, NJ, USA) equipped with a Xenon-arc lamp in 1 nm steps (1 nm bandwidths were chosen for both the excitation and emission monochromators). Fluorescence decays were collected at emission wavelengths from 400 nm to 540 nm with a 10 nm step using an IBH 5000 U SPC spectrometer equipped with an IBH laser diode NanoLED 11 373 nm (IBH, Glasgow, UK) and a cooled Hamamatsu R3809U-50 microchannel plate photomultiplier. The data was analyzed using IBH DAS 6

(IBH, Glasgow, UK) and TRES regeneration script written in Matlab (MATLAB 2010b, MathWorks, Natick, Massachusetts, USA).

2.2. Lipid/polydiacetylene Colorimetric Assay

Lipid/polydiacetylene (PDA) vesicles (PDA/POPC 3:2, mole ratio) were prepared by dissolving the lipid components in chloroform/ethanol and drying together in vacuo. Vesicles were subsequently prepared in DDW by probe-sonication of the aqueous mixture at 70 °C for 3 min. The vesicle solution was then cooled at room temperature for an hour and kept at 4 °C overnight. The vesicles were then polymerized using irradiation at 254 nm for 10–20 s, with the resulting solutions exhibiting an intense blue appearance. PDA fluorescence was measured in 96-well microplates (Greiner Bio-One GmbH, Frickenhausen, Germany) on a Fluoroscan Ascent fluorescence plate reader (Thermo Vantaa, Finland). All measurements were performed at room temperature at 485 nm excitation and 555 nm emission using LP filters with normal slits. Acquisition of data was automatically performed every 5 min for 60 min. Samples comprised 30 μL of POPC/PDA solution and the needed volume of the to be investigated substance followed by addition of 30 μL 50 mM Tris-base buffer (pH 8.0). A quantitative value for the increasing of the fluorescence intensity within the PDA/POPC-labeled vesicles is given by the fluorescence chromatic response (%FCR), which is defined as follows: $\%FCR = [(F_I\text{-}F_0)/F_{100}] \times 100$, where F_I is the fluorescence emission of the lipid/PDA vesicles after addition of the tested membrane-active compounds, F_0 is the fluorescence of the control sample (without addition of the compounds), and F_{100} is the fluorescence of a sample heated to produce the highest fluorescence emission of the red PDA phase minus the fluorescence of the control sample. Chloroform and ethanol were purchased from Bio-Lab Ltd. Jerusalem, Israel. 1-palmitoyl-2-oleoyl-*sn*-glycero-3-phosphocholine (POPC), were purchased from Avanti Lipids (Alabaster, AL, USA). The diacetylenic monomer 10,12-tricosadiynoic acid was purchased from Alfa Aesar (Karlsruhe, Germany).

2.3. Molecular Dynamics Simulations

We performed MD simulations of concentrated aqueous solutions of Arg, Lys, deca-Arg, or deca-Lys in contact with POPC or mixed POPC/POPS bilayers.. The solutions contained 120 individual amino acids or 12 decamers with 0.125 M of NaCl in order to match the

fluorescence experimental conditions. Each of the studied amino acids or peptides was neutralized with an appropriate number of chloride counterions. Bilayers containing 128 POPC lipid molecules or 102 POPC + 26 POPS molecules were constructed such that individual lipids were placed on an 8 x 8 grid resulting in a bilayer of two monolayers each containing 64 individual lipid molecules. In case of mixed POPC/POPS bilayers, 13 POPS lipids were randomly placed in each of the leaflets replacing the same number of POPC molecules. Lipid bilayers were equilibrated until a constant area per lipid was obtained (i.e.,at least 20 ns for the POPC bilayer and 200 ns for the POPC/POPS bilayer). Aminoacids or peptide with counterions and the lipid bilayer were placed together in a unit cell and solvated by approximate 7000 water molecules which were described by the simple point charge (SPC) model.[65] The size of the unit cell was approximately 6.5 x 6.5 x 9.0 nm. Individual amino acids, ions and peptides were described by OPLSAA force field, while POPC and POPS lipid molecules were described using Berger force field. System was set up in a way that the lipid bilayer spaned the *xy* plane and *z* coordinate was normal to the bilayer. 3D periodic boundary conditions were applied with long range electrostatic interactions beyond the nonbonded cutoff of 1 nm accounted for using the particle-mesh Ewald procedure[66] with Fourier spacing of 1.2 nm. The real space Coulomb and van der Waals interactions were cut off at 1 nm. Simulations were performed with the semi-isotropic pressure coupling, independently in the directions parallel and perpendicular to the bilayer normal, employing the Parrinello–Rahman algorithm.[67] Pressure was set to 1 bar and a coupling constant of 2 ps was employed. Temperature of 310 K was controlled with the Nose–Hoover thermostat[68], independently for the lipid, protein, and water sub-systems, with a coupling constant of 1 ps. Bond lengths within lipids and peptide molecules were constrained using the LINCS algorithm.[69] Water bond lengths were kept constant employing the SETTLE method.[70] Equations of motion were integrated using the leap-frog algorithm with a timestep of 2 fs. All the simulated systems were equilibrated for 20 ns, with subsequent 80 ns simulations used for analysis MD simulations were performed with the program package GROMACS, version 4.0.7.[71]

3. Results

3. 1. Neutral zwitterionic POPC vesicles

3.1.1.Time-Dependent Fluorescence Shift

Results of time-dependent fluorescence shift (TDFS) experiments on neutral POPC vesicles labeled with Laurdan or Dtmac dyes upon addition of investigated amino acids or peptides are presented in Table 1. TDFS data (i.e, total spectral shifts $\Delta\nu$ proportional to local polarity, and mean relaxation times τ inversely proportional to local lipid mobility) are listed together with mean values of excitation generalized polarization GP_{EX} (the higher the value of GP_{EX} the more packed/dehydrated the bilayer). Excitation generalized polarization is defined for Laurdan probe as $GP_{EX} = (I_{440}-I_{490})/(I_{440}+I_{490})$, where I_{440} and I_{490} are the fluorescence intensities emitted at 440 and 490 nm. Changes observed to the neutral zwitterionic POPC bilayer upon addition of individual Arg or Lys amino acids are small (i.e., within the error of the measurements) and no significant differences were observed between Arg vs. Lys.

For the deca-peptides and the longer polymers, slightly higher values of Laurdan GP_{EX} and relaxation times τ both for Laurdan and Dtmac compared to peptide free systems, indicate stiffening of the bilayer upon peptide addition. These effects are somewhat more pronounced for the decamers than for longer chain polymers. Here again, as in the case of individual amino acids, no significant differences between Arg and Lys containing peptides were observed.

3.1.2. Molecular Dynamics Simulations

Behavior of individual Arg or Lys amino acids and deca-Arg or deca-Lys peptides at the neutral POPC bilayer was also studied by MD simulations. Figure 3 shows radial distribution functions (RDFs) of POPC choline nitrogen atom (N_4) or POPC phosphate phosphorus atom (P_8) and the guanidinium carbon atom (C_Z) in arginine or ammonium nitrogen atom (N_Z) in lysine containing systems. C_Z atoms are found to come ca. 0.1 nm closer than N_Z atoms to POPC nitrogen N_4 atoms, both for individual amino acids and deca-peptides. The two peaks of unequal height in RDFs describing interaction of C_Z atoms with P_8 atoms in POPC phosphate groups indicate a bimodal (bidentate and monodentate) mode of binding of the guanidinium ($–Gdm^+$) cationic group present in the Arg side chain. Conversely, the binding of the ammonium cationic group ($–NH_3^+$) present in the Lys side chain to the POPC phosphate group is monodentate with only a single peak present in the RDFs. This can be rationalized in terms of the planar $–Gdm^+$ cationic group having different geometry and more hydrogen bond

donors than the tetrahedral $–NH_3^+$ cationic group. This provides the $–Gdm^+$ group in Arg peptides the additional ability to bind the POPC phosphate group with two hydrogen bonds simultaneously resulting in the bidentate binding.

Figure 4 presents number density profiles of the amino acids or peptides, the POPC lipid choline nitrogen atoms (N_4), the POPC lipid phosphate phosphorus atoms (P_8) and water oxygens (OW), along the *z*-coordinate, i.e., as a function of the distance *d* from the POPC bilayer center. Differences in number densities between the individual systems are small, with slightly enhanced densities of Arg and deca-Arg, compared to Lys and deca-Lys in the vicinity of phosphate groups at a distance of ca. 2 nm from the bilayer center. Hydration at the bilayer of Arg-containing systems is also more pronounced as compared to those with Lys as evidenced by the number density of water molecules which follows the Arg density more closely than for Lys. Nevertheless, densities of all peptides at the bilayer are lowered compared to their bulk values (i.e., at distances larger than ~4 nm from the bilayer center), indicating that there is no significant attractive interaction between positively charged peptides and the neutral zwitterionic bilayers in aqueous solutions.

3.2. Negatively charged POPC/POPS vesicles and biomimetic POPC/PDA assays

3.2.1. Time-Dependent Fluorescence Shift

Changes in TDFS spectra observed for the negatively charged POPC/POPS lipid vesicles upon addition of peptides (Table 2) are larger compared to those for neutral POPC vesicles (Table 1).

For individual amino acids, the Laurdan GP_{EX} and relaxation time τ decreases while $\Delta\nu$ slightly increases compared to peptide free systems, which means that the bilayer at the level of lipid carbonyls becomes less dense, more mobile, and slightly more hydrated with the effect being stronger for Arg. In the same systems, the environment around Dtmac probe is slightly dehydrated, especially for Arg which is indicated by a significant decrease of $\Delta\nu$ compared to Lys.

Deca-peptides induce the strongest effects for the Laurdan probe, with very strong dehydration (low $\Delta\nu$ values) and hindrance of local lipid mobility (increased τ values) which is also manifested in elevated GP_{EX} values compared to peptide free systems. In case of deca-Arg, slightly lower τ values compared to deca-Lys indicate that the bilayer is more mobile.

Similar effects, but considerably weaker, are observed for the longer poly-peptides when using the Laurdan probe. On the other hand, at the level of lipid phosphate groups probed by Dtmac probe, significant dehydration is observed only for the longer polymers (lowered Δv values), but not for the deca-peptides where Δv values remain unaltered compared to peptide free systems. This discrepancy between the results obtained at the levels of the phosphate groups (Dtmac) and the carbonyls (Laurdan) indicates deeper penetration of the deca-peptides toward the carbonyls in comparison to longer polymers, which produce the strongest effects at the phosphate level. When using Dtmac probe, no significant differences in TDFS spectra between Arg and Lys containing peptides were observed.

3.2.2. Biomimetic Colorimetric Assays

Figure 5 shows titration curves of individual Arg and Lys amino acids, the two deca-peptides, as well as the corresponding poly-peptides following addition to mixed POPC/PDA vesicles. The dose-response curves in Figure 5 depict the concentration dependence of the percentage fluorescence chromatic response (%FCR) of the vesicle-embedded PDA, which reflects the extent of vesicle surface disruption.[72] Specifically, several studies have correlated the degree of chromatic transformations recorded in PDA-based vesicles with the extent of membrane-interface interactions by membrane-active species.[56] The dose-response curves in Figure 5 underscore significant differences in membrane interaction profiles among the biomolecules examined. In cases of the individual Arg and Lys amino acids, the %FCR response is negligible, which is consistent with a lack of appreciable membrane interactions expected for these small molecules which are soluble in water. In contrast, deca-Arg and poly-Arg displayed steep dose-response curves, pointing to enhanced bilayer surface interactions for these peptides.[73] In case of deca-Lys and poly-Lys, the more moderate %FCR dose-response curve in contrast indicates that the Lys-containing species do not significantly localize onto the bilayer interface.

3.2.3.Molecular Dynamics Simulations

A detailed insight to the molecular structure of the investigated amino acids and peptides at the negatively charged mixed POPC/POPS and POPC/PDA bilayers is provided by MD simulations. Radial distribution functions (RDFs) of the POPC choline nitrogen atom

(N_4(POPC)), the POPS serine nitrogen atom (N_4(POPS)), the POPC phosphate phosphorus atom (P_8), and the POPS phosphate phosphorus atom (P_{11}) around the central carbon atom (C_Z) in arginine and the central nitrogen atom (N_Z) in lysine containing species are presented in Figure 6. First, we note that the presence of negatively charged phospholipids results in a significantly enhanced interactions with all the investigated cationic amino acids and peptides (compare Figures 6 and 3). As for the neutral zwitterionic POPC bilayers (Figure 3), the central carbon C_Z atom in Arg containing peptides is found ca. 0.1 nm closer to POPC choline nitrogen atom N_4 than central nitrogen atom N_Z in lysine containing peptides. This is valid both for individual amino acids and deca-peptides (Figure 6). A similar, bimodal (bidentate and monodentate) binding pattern also exists between POPC phosphate group and $–Gdm^+$ group. Binding of the POPS phosphate group to Gdm^+ group is mostly monodentate, showing only a single pronounced peak in the RDFs. Interestingly, there is an additional peak in RDFs at ca. 3.5 nm between the POPS serine N_4 atom and the central carbon C_Z atom for both Arg and deca-Arg, indicating a close interaction between these two groups. This peak is more pronounced and clearly separated in case of deca-Arg when compared to Arg. In case of Lys and deca-Lys, binding to POPC and POPS phosphate groups is monodentate, but stronger than in case of Arg and deca-Arg. As in the case of the neutral zwitterionic POPC vesicles (Figure 3), the peak between the central nitrogen atom N_Z of the $–NH_3^+$ group and POPC and POPS phosphate groups is shifted by ca. 0.1 nm to larger distances compared to that of the $–Gdm^+$ group (Figure 6). In order to rule out the initial conditions bias, additional simulations starting from different initial conditions were performed for the system Arg/POPC+POPS which showed no qualitative difference in the shape of RDFs.

Number densities of amino acids, peptides, the POPC choline nitrogen atoms (N_4(POPC)), the POPS serine nitrogen atoms (N_4(POPS)), the POPC phosphate phosphorus atoms (P_8), the POPS phosphate phosphorus atom (P_{11}), and water vs. distance from the POPC/POPS bilayer center are presented in Figure 7. In contrast to the neutral zwitterionic POPC bilayer, there is an enhanced density of all studied peptides at the negatively charged POPC/POPS vesicles, as already evidenced by the RDFs. The density maximum is found just outside the membrane, at a distance of ca. 2.5 – 3.0 nm from the POPC/POPS bilayer center. The enhanced density at the membrane surface is a consequence of favorable electrostatic attraction between the negatively charged POPC/POPS bilayer and the positively charged amino acids and deca-peptides which is not present in case of the neutral zwitterionic POPC bilayer. Detailed inspection of number density profiles reveals that in case of Arg and deca-

Arg there is a thick peptide layer adsorbed at the bilayer surface (from ca. 1.2 nm to 3.5 nm from the bilayer center) with maximum density at a distance of 3.0 nm in case of Arg and 2.5 nm in case of deca-Arg.

In case of Arg, the difference between bulk and surface concentrations is rather small, whereas in case of deca-Arg, this difference is large, indicating strong adsorption to the bilayer. The adsorption layer in Lys containing species is significantly weaker and thinner compared to Arg containing species, spanning the region from ca. 1.5 nm to ca. 3.0 nm from the POPC/POPS bilayer center in both Lys and deca-Lys. Actually, no density peak is found in case of Lys, whereas the maximum number density is found at the distance of ca. 2.5 nm in case of deca-Lys. We should mention that these results are not fully converged due to strong adsorption of positively charged peptides at the bilayers. As a result, little exchange with peptides in the water phase was observed at the simulation time scale. Nevertheless, the present simulations qualitatively capture the different membrane adsorption of Arg- vs. Lys-containing species and quantitatively describe binding patterns of Arg and Lys rich peptides at lipid headgroups.

4. Discussion

The effects of Arg and Lys containing peptides on the neutral zwitterionic POPC bilayers are very small. This is reflected in small differences in experimental TDFS results (Table 1), as well as in the number densities obtained from MD simulations for individual amino acids and deca-peptides, showing little peptide adsorption at the membrane (Figure 4). RDFs (Figure 3) show that the binding of the Arg side chain $–Gdm^+$ group to the negative POPC phosphate group is bidentate, whereas the binding of the Lys side chain $–NH_3^+$ group is monodentate, due to the geometry differences between these side chain groups. Interestingly, the Gdm^+ group is found ca. 0.1 nm closer to the positively charged POPC choline group than the $–NH_3^+$ group. These differences in binding pattern between Arg and Lys containing peptides, however, affect only weakly their membrane affinities due to the lack of a strong attractive Coulombic interactions to neutral, zwitterionic POPC bilayers.

In case of negatively charged POPC/POPS or POPC/PDA vesicles, peptide adsorption as well as differences between individual species are significantly larger due to enhanced electrostatic interactions between positively charged peptides and negatively charged bilayers. This is seen first in TDFS spectra for POPC/POPS vesicles, where the largest difference is

observed for deca-peptides which interact most strongly with the bilayer making it less hydrated (lower $\Delta\nu$ values) and less mobile (increased τ values) at the lipid carbonyl level, compared to free vesicles and also to systems with individual amino acids and polymers. The differences in penetration abilities are also demonstrated by the comparison of results obtained with two fluorescent probes (Laurdan and Dtmac) which monitor lipid mobility and polarity around the lipids at different depths (Table 2). In case of deca-peptides, lack of dehydration around lipid phosphate groups closer to the surface (monitored by the Dtmac probe), but not around the carbonyls (probed by Laurdan) indicates their increased penetration ability compared to individual amino acids and polymers. At this point, it has not been possible to run direct MD simulations long enough to directly confirm the deeper penetration of deca-peptides compared to individual Arg and Lys amino acids, but in the future we plan to set up free energy calculations to further address this issue.

Analysis of the fluorescent response induced upon addition of the tested molecules to POPC/PDA vesicles reveals a steep dose curve for deca-Arg and poly-Arg (Figure 5) underscoring their strong interactions with the membrane surface. In comparison, in cases of deca-Lys and poly-Lys the %FCR response curves are less steep, indicating a weaker interaction with the membrane surface. In order to demonstrate why deca-Arg and poly-Arg induce strong interactions with the bilayer surface in contrast to deca-Lys and poly-Lys, representative MD snapshots of deca-Arg and deca-Lys in the vicinity of negatively charged POPC/POPS vesicles are presented in Figure 8. Analysis of selected snapshots shows that deca-Arg peptides have the tendency to form aggregates at the bilayer surface in contrast to deca-Lys. A similar behavior was also observed at the surface of zwitterionic POPC vesicles although to a lesser extent due to the lack of strong attractive electrostatic interactions. We infer that the deca-Arg and poly-Arg aggregation at the bilayer interface accounts for significantly stronger FCR signal at the negatively charged POPC/PDA vesicles. Since the deca-Arg aggregates possess at least a doubled amount of positive charge (+20 for a dimer compared to +10 for a monomer), it can be expected for these aggregates that interactions with negatively charged bilayers will be stronger. Also these aggregates lead to larger transmembrane electric fields inducing stronger perturbations in the bilayer.[19,74] Similar results have already been noted earlier in atomistic MD studies of penetration of antimicrobial penetratin peptides, where an aggregated peptide cluster played the role of a trigger for large membrane deformations, suggesting that energy independent micropinocytosis could be one of the mechanisms of peptide translocation through membranes.[45] Coarse grained MD

simulations have also suggested that larger amounts of adsorbed particles increase membrane surface coverage and increased binding energies then can facilitate passive macropinocytosis.[47] Therefore, the aggregation of deca-Arg could be a decisive factor in more efficient adsorption of deca-Arg peptides at the membrane surface and their consequent penetration into the bilayer. Considerable thinning by ca. 10 % and 12% upon the deca-Arg adsorption was also observed for both neutral and negatively charged bilayers, respectively, which could also lower the energy barrier for penetration.

It is also interesting to look in more detail at the deca-Arg aggregates at the negatively charged POPC/POPS vesicle in order to elucidate the reasons behind the unusual stability of the deca-Arg dimer and larger clusters. We see from Figure 9 that the deca-Arg dimer is remarkably stabilized due to several factors. First, there are two strong bidentate salt-bridge attractive interactions between positive side chain $–Gdm^+$ groups and the negatively charged C-terminus of the other peptide. In addition, slightly attractive interactions between like charged $–Gdm^+$ groups contribute to the aggregate stability as well. The unintuitive like charge Gdm^+ pairing has been observed earlier in a number of protein structures,[75,76] electrophoretic measurements[77] and several recent theoretical studies including classical and *ab initio* MD studies.[78-81] We proposed that it occurs primarily due to dispersion and quadrupolar effects and stabilizing hydrophobic interactions between planar disc-shaped Gdm^+ cations in water (with lack of these interactions in case of NH_4^+ cations).[79-81] In case of deca-Lys, an analogous like charge pairing between side chain $–NH_3^+$ groups is not observed and, consequently, during the present MD simulations dimers are formed neither in the water phase, nor at the membrane surface.

In summary, we have obtained two independent sets of experimental results corroborated by the peptide-lipid binding patterns obtained from MD simulations. Time-dependent fluorescence shift studies indicate that deca-peptides penetrate deeper in the lipid bilayer than individual amino acids and longer poly-peptides. It is important to note that TDFS is not sensitive to peptide aggregation per se, since the fluorescence signal obtained from large ensemble of probe molecules is averaged. The mean hydration and mobility probed by Laurdan and Dtmac molecules were apparently not influenced by the deca-arginine aggregation. It is likely that any pronounced changes in the TDFS signal due to locally increased deca-arginine concentrations would be compensated by the signal from the bilayer areas with lower peptide concentration. Therefore, the TDFS results are not contradictory but rather complementary to the results of the colorimetric assay. In contrast, biomimetic

colorimetric assays show that deca-Arg and poly-Arg induce strong interactions with the bilayer surface. MD simulations confirm this and suggest that these interactions are due to the aggregation of deca-Arg at the surface. In case of poly-Arg the aggregation effect at the membrane surface is also strong, but it is unlikely that very long peptide aggregates efficiently penetrate into the bilayer due to their large size, as demonstrated by present TDFS results (Table 2).

Enhanced adsorption and aggregation of deca-Arg at negatively charged bilayers is not the only requirement for explaining the enhanced penetration ability of deca-Arg through the bilayer. Recent coarse grained MD simulations of nona-arginine translocation through asymmetric DMPC/DMPS bilayers have actually shown that the energy barrier for a single nona-arginine is around 20 kcal/mol upon translocating through neutral DMPC leaflet of the bilayer, whereas the barrier for the translocation through negatively charged DMPC/DMPS bilayer is twice as large, being 40 kcal/mol.[82] Although these results are obtained with a coarse grained model, it is not surprising that the latter barrier is larger due to the stronger adsorption of individual positively charged oligoarginine molecules to the negatively charged bilayer leaflet, which is in accord with the results presented in this study. Since the energy barrier for penetration of single arginine amino acid through neutral and negatively charged amino acids are comparable,[40] the enhancement in the adsorption of oligoarginine to the negatively charged bilayer is due to the elongation of the oligopeptide chain. We can speculate that the adsorption of oligoarginine aggregates at the negatively charged bilayers can actually create a kind of reduced charge oligoarginine-negative phospholipid domains[14,83] from which the translocation through the bilayer would be facilitated by reducing the energy barrier height for penetration into the membrane. It remains to be difficult to obtain properly converged atomistic direct MD and free energy data which would capture all molecular properties of Arg and Lys side chain groups. Our future work will be focused on large scale calculations of translocation kinetic parameters of Arg and Lys rich peptides in various phospholipid bilayers in order to further elucidate the translocation ability of oligoarginines.

5. Conclusion

Combination of results obtained from time-dependent fluorescence shift method, biomimetic colorimetric assays, and molecular dynamics simulations helps to understand why arginine rich peptides with intermediate lengths translocate well through cellular membranes

in contrast to lysine rich peptides. Our results show that an important prerequisite for efficient peptide adsorption and, consequently, translocation through membranes is the presence of negatively charged phospholipids, which is the case for many cellular membranes. The second prerequisite is a distinct tendency of adsorbed arginine molecules to aggregate at the bilayer (in contrast to oligolysines) which increases membrane-surface interactions due to the increased effective charge of the aggregates. As adsorption and aggregation of oligoarginines gets stronger by increasing oligomer length, the interactions with the bilayer surface get more pronounced and the lipid bilayer becomes more mobile, as shown for the case of deca-arginine in this study. However, further elongation of the adsorbed peptides hinders efficient penetration deep into the bilayer, which in turn could reduce the translocation ability.

Acknowledgements

M.V. acknowledges support by the Ministry of Science and Technology of Croatia through the project 098-0982933-2920. P.J. thanks the Czech Ministry of Education (grant no. LH12001) for support and acknowledges the Academy of Finland for the FiDiPro award and the Academy of Sciences of the Czech Republic for the Praemium Academie award. Support from the Czech Science Foundation via grant P208/12/G016 is acknowledged. Additionally, M.H acknowledges the Praemium Academie Award (Academy of Sciences of the Czech Republic).

References

(1) Vives, E.; Brodin, P.; Lebleu, B. *J. Biol. Chem.* **1997**, *272*, 16010.

(2) Futaki, S. *Adv. Drug Delivery Rev.* **2005**, *57*, 547.

(3) Fuchs, S. M.; Raines, R. T. *Cell. Mol. Life Sci.* **2006**, *63*, 1819.

(4) Magzoub, M.; Graslund, A. *Q. Rev. Biophys.* **2004**, *37*, 147.

(5) Eguchi, A.; Akuta, T.; Okuyama, H.; Senda, T.; Yokoi, H.; Inokuchi, H.; Fujita, S.; Hayakawa, T.; Takeda, K.; Hasegawa, M.; Nakanishi, M. *J. Biol. Chem.* **2001**, *276*, 26204.

(6) Gratton, J. P.; Yu, J.; Griffith, J. W.; Babbitt, R. W.; Scotland, R. S.; Hickey, R.; Giordano, F. J.; Sessa, W. C. *Nat. Med. (N. Y., NY, U. S.)* **2003**, *9*, 357.

(7) El-Sayed, A.; Futaki, S.; Harashima, H. *AAPS Journal* **2009**, *11*, 13.

(8) Futaki, S.; Suzuki, T.; Ohashi, W.; Yagami, T.; Tanaka, S.; Ueda, K.; Sugiura, Y. *J. Biol. Chem.* **2001**, *276*, 5836.

(9) Schwarze, S. R.; Ho, A.; Vocero-Akbani, A.; Dowdy, S. F. *Science* **1999**, *285*, 1569.

(10) Xu, Y.; Liu, B. R.; Lee, H. J.; Shannon, K. B.; Winiarz, J. G.; Wang, T. C.; Chiang, H. J.; Huang, Y. W. *J. Biomed. Biotehnol.* **2010**, *2010*, 948543.

(11) Liu, B. R.; Li, J. F.; Lu, S. W.; Leel, H. J.; Huang, Y. W.; Shannon, K. B.; Aronstam, R. S. *J. Nanosci. Nanotechnol.* **2010**, *10*, 6534.

(12) Liu, B. R.; Huang, Y. W.; Winiarz, J. G.; Chiang, H. J.; Lee, H. J. *Biomaterials* **2011**, *32*, 3520.

(13) Torchilin, V. P. In *Annu. Rev. Biomed. Eng.*; Yarmush, M. L., Ed., 2006; Vol. 8; pp 343.

(14) Sakai, N.; Matile, S. *J. Am. Chem. Soc.* **2003**, *125*, 14348.

(15) Wender, P. A.; Mitchell, D. J.; Pattabiraman, K.; Pelkey, E. T.; Steinman, L.; Rothbard, J. B. *Proc. Natl. Acad. Sci. U. S. A.* **2000**, *97*, 13003.

(16) Mitchell, D. J.; Steinman, L.; Kim, D. T.; Fathman, C. G.; Rothbard, J. B. *J. Pept. Res.* **2000**, *56*, 318.

(17) Derossi, D.; Calvet, S.; Trembleau, A.; Brunissen, A.; Chassaing, G.; Prochiantz, A. *J. Biol. Chem.* **1996**, *271*, 18188.

(18) Prochiantz, A. *Curr. Opin. Neurobiol.* **1996**, *6*, 629.

(19) Binder, H.; Lindblom, G. *Biophys. J.* **2003**, *85*, 982.

(20) Rothbard, J. B.; Jessop, T. C.; Lewis, R. S.; Murray, B. A.; Wender, P. A. *J. Am. Chem. Soc.* **2004**, *126*, 9506.

(21) Rothbard, J. B.; Jessop, T. C.; Wender, P. A. *Adv. Drug Delivery Rev.* **2005**, *57*, 495.

(22) Richard, J. P.; Melikov, K.; Vives, E.; Ramos, C.; Verbeure, B.; Gait, M. J.; Chernomordik, L. V.; Lebleu, B. *J. Biol. Chem.* **2003**, *278*, 585.

(23) Thoren, P. E. G.; Persson, D.; Esbjoerner, E. K.; Goksoer, M.; Lincoln, P.; Norden, B. *Biochemistry* **2004**, *43*, 3471.

(24) Fischer, R.; Fotin-Mleczek, M.; Hufnagel, H.; Brock, R. *ChemBioChem* **2005**, *6*, 2126.

(25) Chauhan, A.; Tikoo, A.; Kapur, A. K.; Singh, M. *J. Controlled Release* **2007**, *117*, 148.

(26) Amand, H. L.; Fant, K.; Norden, B.; Esbjoerner, E. K. *Biochem. Biophys. Res. Commun.* **2008**, *371*, 621.

(27) Sakai, N.; Takeuchi, T.; Futaki, S.; Matile, S. *ChemBioChem* **2005**, *6*, 114.

(28) Tang, M.; Waring, A. J.; Hong, M. *J. Am. Chem. Soc.* **2007**, *129*, 11438.

(29) Tang, M.; Waring, A. J.; Lehrer, R. I.; Hong, M. *Angew. Chem., Int. Ed. Engl.* **2008**, *47*, 3202.

(30) Sakai, N.; Futaki, S.; Matile, S. *Soft Matter* **2006**, *2*, 636.

(31) Goncalves, E.; Kitas, E.; Seelig, J. *Biochemistry* **2005**, *44*, 2692.

(32) Walrant, A.; Correia, I.; Jiao, C. Y.; Lequin, O.; Bent, E. H.; Goasdoue, N.; Lacombe, C.; Chassaing, G.; Sagan, S.; Alves, I. D. *Biochim. Biophys. Acta, Biomembr.* **2011**, *1808*, 382.

(33) He, J.; Hristova, K.; Wimley, W. C. *Angew. Chem., Int. Ed. Engl.* **2012**, *51*, 7150.

(34) Marks, J. R.; Placone, J.; Hristova, K.; Wimley, W. C. *J. Am. Chem. Soc.* **2011**, *133*, 8995.

(35) Hessa, T.; Kim, H.; Bihlmaier, K.; Lundin, C.; Boekel, J.; Andersson, H.; Nilsson, I.; White, S. H.; Von Heijne, G. *Nature* **2005**, *433*, 377.

(36) MacCallum, J. L.; Bennett, W. F. D.; Tieleman, D. P. *Journal of General Physiology* **2007**, *129*, 371.

(37) Vorobyov, I.; Li, L.; Allen, T. W. *J. Phys. Chem. B* **2008**, *112*, 9588.

(38) Li, L.; Vorobyov, I.; Allen, T. W. *J. Phys. Chem. B* **2008**, *112*, 9574.

(39) Johansson, A. C. V.; Lindahl, E. *J. Chem. Phys.* **2009**, *130*, 185101.

(40) Vorobyov, I.; Allen, T. W. *Biochim. Biophys. Acta, Biomembr.* **2011**, *1808*, 1673.

(41) Schow, E.; Freites, J.; Cheng, P.; Bernsel, A.; von Heijne, G.; White, S.; Tobias, D. *J. Membr. Biol.* **2011**, *239*, 35.

(42) Rychkova, A.; Warshel, A. *Proc. Natl. Acad. Sci. U. S. A.* **2013**, *110*, 495.

(43) Herce, H. D.; Garcia, A. E. *Proc. Natl. Acad. Sci. U. S. A.* **2007**, *104*, 20805.

(44) Herce, H. D.; Garcia, A. E.; Litt, J.; Kane, R. S.; Martin, P.; Enrique, N.; Rebolledo, A.; Milesi, V. *Biophys. J.* **2009**, *97*, 1917.

(45) Yesylevskyy, S.; Marrink, S. J.; Mark, A. E. *Biophys. J.* **2009**, *97*, 40.

(46) Huang, K.; García, Angel E. *Biophys. J.* **2013**, *104*, 412.

(47) Vacha, R.; Martinez-Veracoechea, F. J.; Frenkel, D. *Nano Lett.* **2011**, *11*, 5391.

(48) van Meer, G.; Voelker, D. R.; Feigenson, G. W. *Nat. Rev. Mol. Cell Biol.* **2008**, *9*, 112.

(49) Van Meer, G.; De Kroon, A. I. P. M. *J. Cell Sci.* **2011**, *124*, 5.

(50) Carpick, R. W.; Sasaki, D. Y.; Marcus, M. S.; Eriksson, M. A.; Burns, A. R. *J. Phys.: Condens. Matter* **2004**, *16*, R679.

(51) Charych, D. H.; Nagy, J. O.; Spevak, W.; Bednarski, M. D. *Science* **1993**, *261*, 585.

(52) Kim, J.; Kim, J. M.; Ahn, D. J. *Macromol. Res.* **2006**, *14*, 478.

(53) Orynbayeva, Z.; Kolusheva, S.; Livneh, E.; Lichtenshtein, A.; Nathan, I.; Jelinek, R. *Angew. Chem., Int. Ed. Engl.* **2005**, *44*, 1092.

(54) Kolusheva, S.; Boyer, L.; Jelinek, R. *Nat. Biotechnol.* **2000**, *18*, 225.

(55) Park, C. K.; Kang, C. D.; Sim, S. J. *Biotechnol. J.* **2008**, *3*, 687.

(56) Jelinek, R.; Kolusheva, S. *Biotech. Adv.* **2001**, *19*, 109.

(57) Jurkiewicz, P.; Cwiklik, L.; Jungwirth, P.; Hof, M. *Biochimie* **2012**, *94*, 26.

(58) Hutterer, R.; Schneider, F. W.; Hermens, W. T.; Wagenvoord, R.; Hof, M. *Biochim. Biophys. Acta* **1998**, *1414*, 155.

(59) Horng, M. L.; Gardecki, J. A.; Papazyan, A.; Maroncelli, M. *J. Phys. Chem.* **1995**, *99*, 17311.

(60) Berger, O.; Edholm, O.; Jahnig, F. *Biophys. J.* **1997**, *72*, 2002.

(61) Jurkiewicz, P.; Olzynska, A.; Langner, M.; Hof, M. *Langmuir* **2006**, *22*, 8741.

(62) Olzynska, A.; Zan, A.; Jurkiewicz, P.; Sykora, J.; Grobner, G.; Langner, M.; Hof, M. *Chem. Phys. Lipids* **2007**, *147*, 69.

(63) Barucha-Kraszewska, J.; Kraszewski, S.; Jurkiewicz, P.; Ramseyer, C.; Hof, M. *Biochim. Biophys. Acta, Biomembr.* **2010**, *1798*, 1724.

(64) Epand, R. F.; Kraayenhof, R.; Sterk, G. J.; Sang, H.; Epand, R. M. *Biochim. Biophys. Acta, Biomembr.* **1996**, *1284*, 191.

(65) Berendsen, H. J. C.; Grigera, J. R.; Straatsma, T. P. *J. Phys. Chem.* **1987**, *91*, 6269.

(66) Essmann, U.; Perera, L.; Berkowitz, M. L.; Darden, T.; Lee, H.; Pedersen, L. G. *J. Chem. Phys.* **1995**, *103*, 8577.

(67) Parrinello, M.; Rahman, A. *J. Appl. Phys.* **1981**, *52*, 7182.

(68) Nose, S. *Mol. Phys.* **1984**, *52*, 255.

(69) Hess, B.; Bekker, H.; Berendsen, H. J. C.; Fraaije, J. G. E. M. *J. Comp. Chem.* **1997**, *18*, 1463.

(70) Hockney, R. W.; Goel, S. P.; Eastwood, J. *J. Comp. Phys.* **1974**, *14*, 148.

(71) Hess, B.; Kutzner, C.; van der Spoel, D.; Lindahl, E. *J. Chem. Theory Comp.* **2008**, *4*, 435.

(72) Kolusheva, S.; Shahal, T.; Jelinek, R. *Biochemistry* **2000**, *39*, 15851.

(73) Katz, M.; Ben-Shlush, I.; Kolusheva, S.; Jelinek, R. *Pharm. Res.* **2006**, *23*, 580.

(74) Cahill, K. *Physical Biology* **2010**, *7*.

(75) Sumowski, C. V.; Schmitt, B. B. T.; Schweizer, S.; Ochsenfeld, C. *Angew. Chem., Int. Ed. Engl.* **2010**, *49*, 9951.

(76) Pednekar, D.; Tendulkar, A.; Durani, S. *Proteins: Struct., Funct., Bioinf.* **2009**, *74*, 155.

(77) Kubickova, A.; Krizek, T.; Coufal, P.; Wernersson, E.; Heyda, J.; Jungwirth, P. *J. Phys. Chem. Lett.* **2011**, *2*, 1387.

(78) Masunov, A. m.; Lazaridis, T. *J. Am. Chem. Soc.* **2003**, *125*, 1722.

(79) Vazdar, M.; Vymetal, J.; Heyda, J.; Vondrasek, J.; Jungwirth, P. *J. Phys. Chem. A* **2011**, *115*, 11193.

(80) Vazdar, M.; Uhlig, F.; Jungwirth, P. *J. Phys. Chem. Lett.* **2012**, *3*, 2021.

(81) Vondrášek, J.; Mason, P. E.; Heyda, J.; Collins, K. D.; Jungwirth, P. *J. Phys. Chem. B* **2009**, *113*, 9041.

(82) Li, Z. L.; Ding, H. M.; Ma, Y. Q. *Soft Matter* **2013**, *9*, 1281.

(83) Dietrich, U.; Krueger, P.; Kaes, J. A. *Chem. Phys. Lipids* **2011**, *164*, 266.

Figure Captions

Figure 1. Chemical structures of the investigated Arg and Lys rich peptides (upper panel) and the PDA subunit (lower panel) of the POPC/PDA biomimetic assay.

Figure 2. Chemical structures of the probes included in the POPC and POPC/POPS bilayer showing their approximate location.

Figure 3. Radial distribution functions of selected groups around central carbon atom C_Z (Arg, deca-Arg) and central nitrogen atom N_Z (Lys and deca-Lys), respectively, at the neutral zwitterionic POPC bilayer.

Figure 4. Number densities of selected groups in Arg, deca-Arg, Lys and deca-Lys, respectively, calculated from the center of the neutral zwitterionic POPC bilayer.

Figure 5. Chromatic lipid/PDA membrane assay. Concentration dependence of the percentage fluorescence chromatic response (%FCR). Measurements were carried out after incubating the tested molecules with POPC/PDA vesicles for 60 minutes at room temperature. Poly-arginine (i), deca-arginine (ii), poly-lysine (iii), deca-lysine (iv), arginine (v), lysine (vi).

Figure 6. Radial distribution functions of selected groups around central carbon atom C_Z (Arg and deca-Arg) and central nitrogen atom N_Z (Lys and deca-Lys), respectively, at the negatively charged POPC/POPS bilayer.

Figure 7. Number densities of selected groups in Arg, deca-Arg, Lys and deca-Lys, respectively, calculated from the center of the negatively charged POPC/POPS bilayer.

Figure 8. Selected snapshots from molecular dynamics simulations of deca-Arg (top) and deca-Lys (bottom) peptides at the negatively charged POPC/POPS bilayer. An aggregate of three deca-Arg peptides is shown in red, blue and green color (top). A single adsorbed deca-Lys peptide is shown in blue color (bottom).

Figure 9. Selected snapshot from molecular dynamics simulations of deca-Arg showing a dimer structure stabilized by two salt-bridges and like-charge ion pairing.

Tables

Table 1. Time-dependent fluorescence shift parameters obtained with two different fluorescent probes (Laurdan and Dtmac) at neutral zwitterionic POPC vesicles.

lipid	peptide	GP_{EX}	Laurdan			Dtmac		
			$\Delta\nu$ (cm^{-1}) ± 50	τ (ns) ± 0.05	% obs	$\Delta\nu$ (cm^{-1}) ± 50	τ (ns) ± 0.05	% obs
POPC	-	0.030 ± 0.005	3975	3.18	78%	1925	0.56	44%
	Lys	0.041 ± 0.003	3975	3.16	80%	1925	0.59	45%
	Arg	0.038 ± 0.003	3950	3.16	79%	1900	0.50	47%
	deca-Lys	0.047 ± 0.003	3975	3.21	80%	1975	0.62	49%
	deca-Arg	0.046 ± 0.002	3975	3.24	80%	1975	0.65	59%
	poly-Lys	0.042 ± 0.007	3975	3.21	79%	1950	0.53	52%
	poly-Arg	0.045 ± 0.004	3950	3.19	79%	1975	0.64	46%

Table 2. Time-dependent fluorescence shift parameters obtained with two different fluorescent probes (Laurdan and Dtmac) at negatively charged POPC/POPS bilayer.

lipid	peptide	Laurdan				Dtmac		
		GP_{EX}	$\Delta\nu$ (cm^{-1}) ± 50	τ (ns) ± 0.05	% obs	$\Delta\nu$ (cm^{-1}) ± 50	τ (ns) ± 0.05	% obs
POPC/POPS	-	0.072 ± 0.002	3850	3.50	80%	2075	0.59	63%
	Lys	0.068 ± 0.004	3900	3.34	79%	2025	0.60	62%
	Arg	0.038 ± 0.005	3900	3.16	80%	1950	0.55	57%
	deca-Lys	0.137 ± 0.003	3625	4.19	80%	2050	0.61	62%
	deca-Arg	0.136 ± 0.006	3675	4.01	81%	2025	0.56	60%
	poly-Lys	0.098 ± 0.002	3775	3.68	81%	1975	0.57	61%
	poly-Arg	0.096 ± 0.002	3775	3.87	81%	1950	0.56	60%

Figures

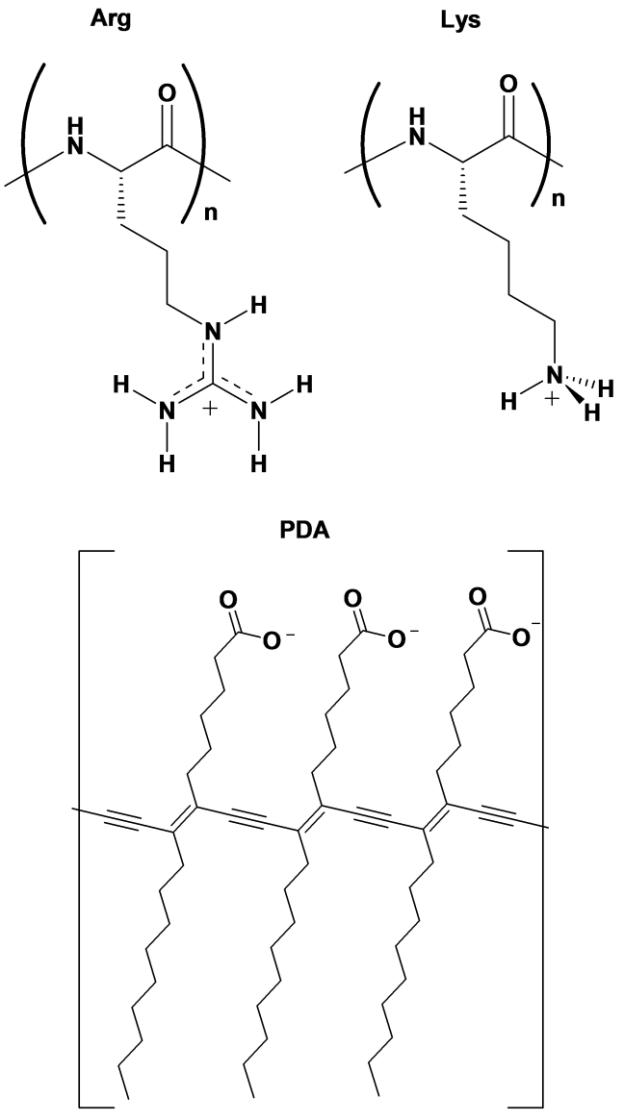

Figure 1.

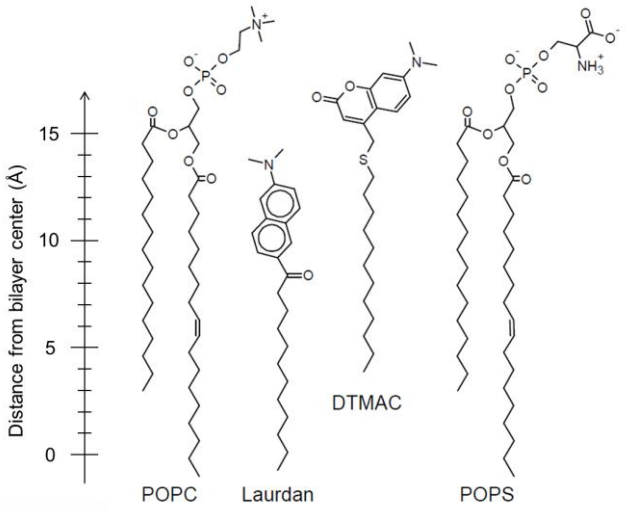
Distance from bilayer center (Å)
15
10
5
0
POPC
Laurdan
DTMAC
POPS

Figure 2.

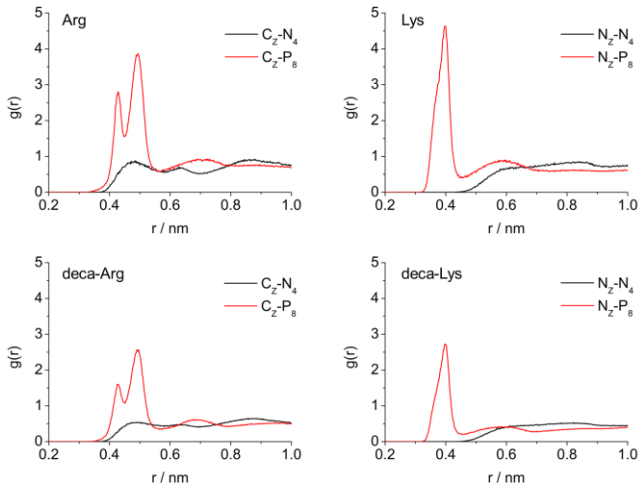
Arg
C_Z-N_4
C_Z-P_8
Lys
N_Z-N_4
N_Z-P_8
deca-Arg
C_Z-N_4
C_Z-P_8
deca-Lys
N_Z-N_4
N_Z-P_8
g(r)
r / nm
0
1
2
3
4
5
0.2
0.4
0.6
0.8
1.0

Figure 3.

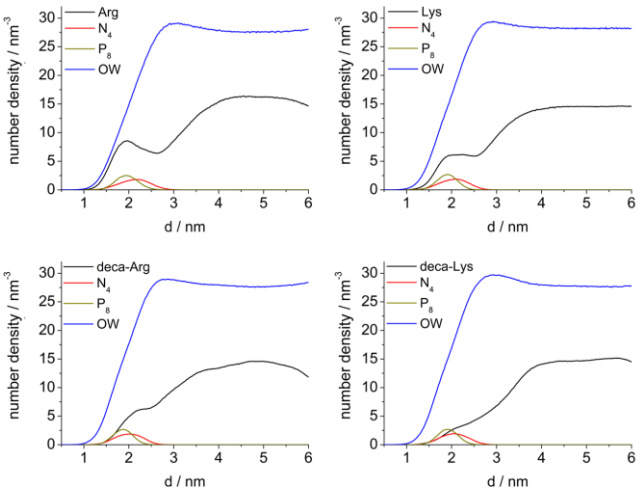

Figure 4.

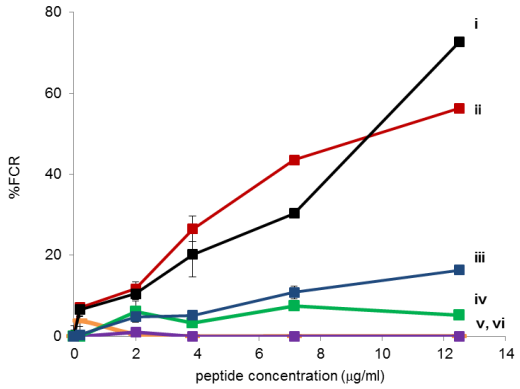
80
60
40
20
0
%FCR
0
2
4
6
8
10
12
14
peptide concentration (µg/ml)
i
ii
iii
iv
v, vi

Figure 5.

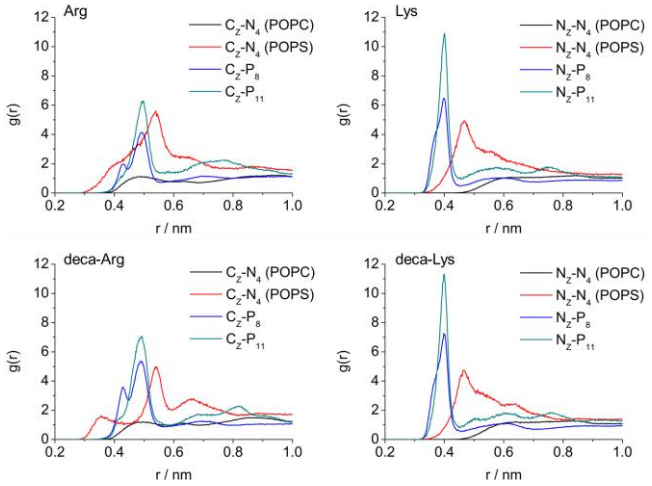
Arg
Lys
deca-Arg
deca-Lys
g(r)
r / nm
C_Z-N_4 (POPC)
C_Z-N_4 (POPS)
C_Z-P_8
C_Z-P_11
N_Z-N_4 (POPC)
N_Z-N_4 (POPS)
N_Z-P_8
N_Z-P_11

Figure 6.

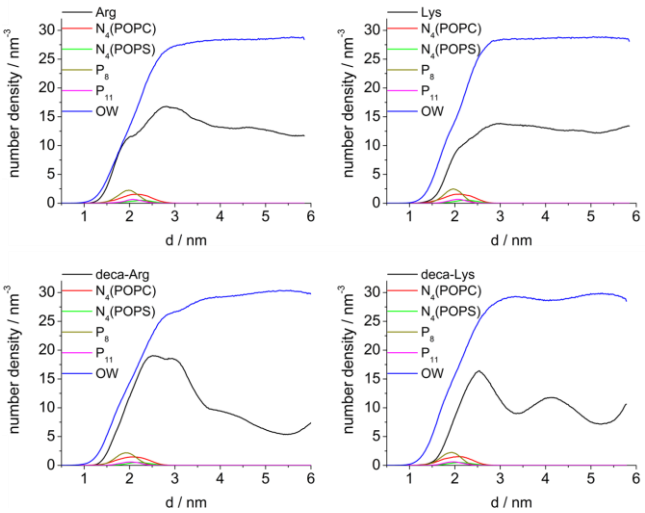
Arg
Lys
deca-Arg
deca-Lys
N4(POPC)
N4(POPS)
P8
P11
OW
number density / nm-3
d / nm

Figure 7.

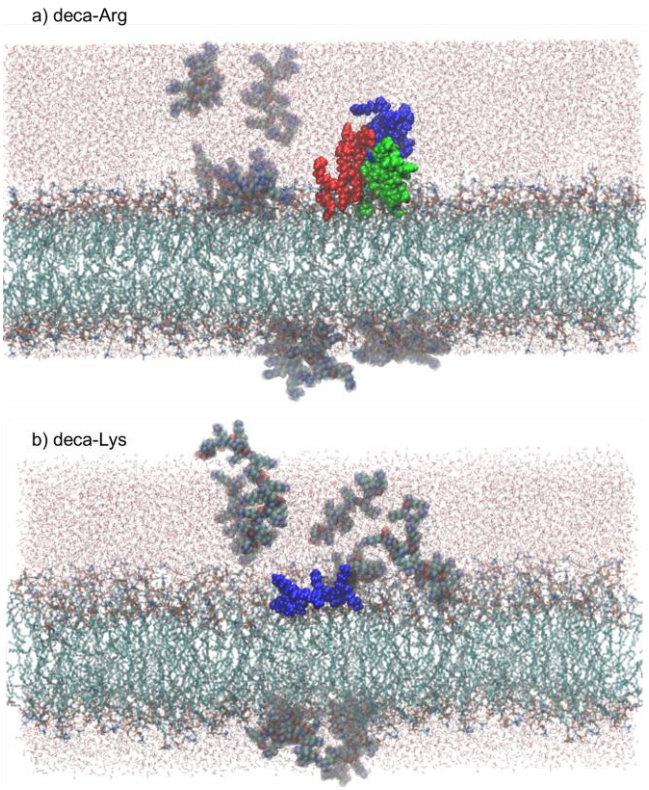

Figure 8.

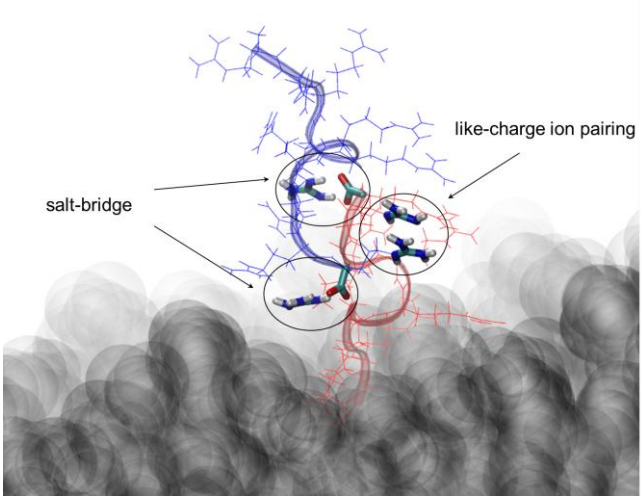

Figure 9.

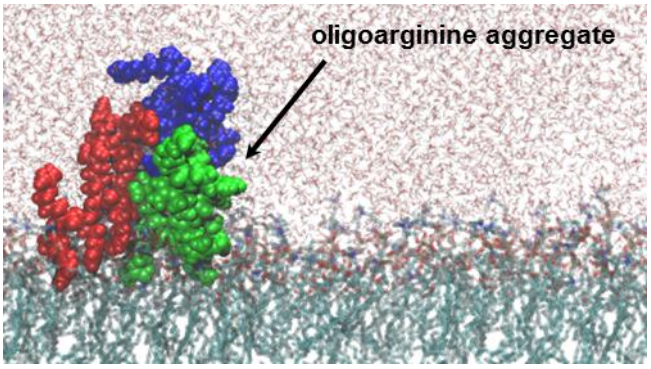

TOC graphics